The Report committee for Marco Gulino
Certifies that this is the approved version of the following report:

A Homotopic Approach to Solve the Fuel Optimal Spacecraft Proximity Operations Problem

APPROVED BY

SUPERVISING COMMITTEE:

Maruthi R. Akella, Supervisor

Efstathios Bakolas

A Homotopic Approach to Solve the Fuel Optimal Spacecraft Proximity Operations Problem

by

Marco Gulino, B.S.; M.S.; M.S.

REPORT

Presented to the Faculty of the Graduate School of

The University of Texas at Austin

in Partial Fulfillment

of the Requirements

for the Degree of

MASTER OF SCIENCE IN ENGINEERING

The University of Texas at Austin

May 2017

Dedicated to my father.

Acknowledgments

I would like to thank Dr Akella and Dr Bakolas for the relevant and helpful comments provided during the preparation of this report and more in general during my research at UT. I deeply appreciate the availability and the knowledge they showed and shared with me. Moreover I am thankful to Dr Bakolas for having initiated me to the field of optimal control which I came to love.

Moreover I am profoundly grateful to the Fulbright Commission for having funded part of my program at UT. Without their support I would have not been able to embark in this fantastic journey where I had the chance to expand my knowledge in ways I did not foresee and to know and confront myself with people coming from all over the World.

My appreciation goes to my fellow researchers of the C-DUS lab with whom I had many stimulating conversations ranging from science to basically whatever topic one can think of. My learning and social experience would have not been so amazing without them.

Last but not least, I am extremely grateful to have my family besides me that was able to support me in this journey made of curiosity satisfaction and hard work. I am particularly thankful to my wife Sara who helped me greatly in facing the difficulties annexed with learning and with doing research.

A Homotopic Approach to Solve the Fuel Optimal Spacecraft Proximity Operations Problem

by

Marco Gulino, M.S.E.
The University of Texas at Austin, 2017

Supervisor: Maruthi R. Akella

This report focuses on finding the low-thrust fuel optimal solution to a class of spacecraft proximity operations subject to path constraints. The mission is for a service spacecraft to perform a surveying orbit relative to a reference within a prescribed period, without violating a no fly zone represented by a sphere centered on the reference vehicle. Clohessy-Wiltshire equations are used, together with the controllability Gramian of the resulting linear system, to obtain an analytical solution to the energy optimal problem. A homotopic approach is subsequently shown to serve as an effective bridge from the energy optimal solution toward the fuel optimal solution.

Table of Contents

List of Tables

List of Figures

Chapter 1

Introduction

Spacecraft rendezvous and proximity operations have acquired increasing attention in the last two decades due to the access to enhanced mission capabilities that such technologies offer. In this framework, having a controller that minimizes fuel consumption is paramount as it allows longer mission durations. Autonomy is also an important capability for a spacecraft as it contributes to reduce operations cost and it allows operating the spacecraft in scenarios where human interaction is not feasible or practical.

When dealing with optimal control problems, the designer has basically two choices on which method to adopt to solve the problem: indirect and direct. As frequently in life, both of these methods have their pros and cons. In direct methods the control inputs itself are the optimization variables. They are usually easier to set up and can prove to be particularly efficient, especially if written in a convex form. However, ensuring lossless convexification is not straightforward in many cases of practical interest. Moreover, direct methods may present accuracy problems. In indirect methods instead, the optimization variables are the costates which are chosen to satisfy the necessary conditions for minimization of the cost function. The costates are then used to define

the optimal control inputs. It is clear then that the optimal control input is indirectly found through the costates, hence the name of the method. Indirect method are harder to set up and can be slower than direct methods, however, since the necessary constraints for optimality are imposed along the whole trajectory, the solution will provide better accuracy.

Extensive work has been performed in this field tackling the problem of fuel optimal trajectory planning using continuous low- and high-thrust with different approaches and for different applications. Typically, rendezvous and docking operations are missions for high-thrust vehicles (*e.g.* ATV, Soyuz) with the purpose of ISS refurbishment. On the other hand, low-thrust is becoming increasingly popular for missions like orbital transfers like in [13], [5], [3] and formation flying [10] for increased mission duration and capability that such a technology is able to offer.

Recently, the fuel optimal rendezvous problem was solved through an indirect method by using continuous [11], [12] and impulsive [1] maneuvers and high-thrust. Kumar and Seywald [9] instead approached the problem of fuel optimal station keeping through a direct method using high-thrust spacecraft.

Low-thrust applications have been analyzed following a similar approach as the one proposed in the present work for a formation flying reconfiguration problem [10]. Atkins, Kolmanovsky and Taheri [3] adopted a clever solution, given by extended logarithmic smoothing of the cost function, to solve challenging fuel optimal interplanetary trajectory problems by also integrating concepts from Li et al. [5] and Alonso et al. [6].

This work focuses on an application for which, to the best of the author knowledge, little work has been done: proximity operations around a reference spacecraft in GEO orbit using a low-thrust service vehicle. The potential application of this capability would be to perform survey orbits around the reference vehicle with the purpose of estimating the need for an intervention or to prepare a subsequent rendezvous. The need for this capability has been already identified and the problem was analyzed from a high-thrust viewpoint [4].

Instead, this work aims to solve a low thrust fuel optimal proximity operations problem through the indirect optimization method, where the mission for the service vechicle is to perform a surveying orbit around a reference spacecraft that is orbiting in a circular orbit about the Earth. Path constraints are imposed to the optimal control problem in order to not violate a no fly zone defined by a sphere of arbitrarily large radius centered on the reference.

The path constraints make it extremely hard to reduce the problem to a two point boundary value problem as it would be necessary to discretize the trajectory in on and off boundary arcs, therefore requiring to know in advance their sequence which is seldom possible. However, using Clohessy-Wiltshire (CW) equations, [2] an analytical solution to the energy optimal problem is obtained. The energy optimal solution is then bridged to the fuel optimal solution through homotopy which has proven to be an effective and powerful approach to find the solution to difficult optimization problems [13], [5], [8], [7], [10]. In the energy optimal solution, the path constraints have been imposed

in a soft way through way points. In the following it will be shown that regions where the fuel optimal solution is safer than the energy optimal solution exist therefore guaranteeing a non-violation of a no fly zone.

This work follows the lines of Xi et al. [10] where a similar approach was applied although for a different application (formation flying), using Tschauner-Hempel equations, and with a different implementation. The singularities, that are endemic to this problem, were solved in that paper by using a recursive homotopic approach based on a non-linear solver. The present work instead bridges energy optimal and fuel optimal solutions by integrating the optimal costates at final time from energy optimal to fuel optimal, while tracking the zero curve given by the shooting function. In this approach, non-linear solvers, which are often source of divergence and solution locality, are bypassed. The proposed approach solves the typical singularities of the problem by raising the precision of the integration of the homotopic procedure by localizing analytically the switching time instants and by evaluating gradients and Jacobians using the method of complex step differentiation.

In the following, first the formulation of the problem will be presented, followed by the homotopic approach proposed by this report. Energy optimal and fuel optimal solutions will follow to arrive to the discussion of the results as a conclusion.

Chapter 2

Formulation of the Problem

Consider a prototype scenario wherein the task is to find the control history (continuous low-thrust) that allows a service spacecraft to perform a surveying orbit (with a given period) about the reference spacecraft that is on a GEO orbit around the Earth while ensuring minimum fuel consumption. For this problem, a 500 kg spacecraft provided with an engine able to deliver 0.1 N of thrust and 1600 seconds of specific impulse has been considered. The author considers the aforementioned sizing credible for a small size spacecraft equipped with electric propulsion.

In first approximation, the dynamics of motion for each spacecraft for the present scenario are driven by two body gravity only and are described by the following equations:

$$\dot{\boldsymbol{r}}(t) = \boldsymbol{v}(t) \tag{2.1}$$

$$\ddot{\boldsymbol{r}}(t) = -\frac{\mu}{r(t)^3}\boldsymbol{r}(t) + \frac{\boldsymbol{F}(t)}{m} \tag{2.2}$$

where $\boldsymbol{r}$ and $\boldsymbol{v}$ are the position and velocity vectors expressed in the reference frame centered on Earth and $\boldsymbol{F}$ is the thrust vector of the spacecraft considered.

In the following, a few assumptions will be observed. The mass of the service spacecraft will be considered constant because, as will be clear in the

following, the mass used for each maneuver is negligible (a few tens of grams) with respect to the total mass of the spacecraft (500 kg), thus resulting in an acceleration that can be considered constant in first approximation. The reference and the service spacecraft will not be affected by third body and non central perturbations because the duration of the maneuvers will be short compared to the duration of 1 orbit of the reference spacecraft. Labeling $\boldsymbol{r^*}$ the

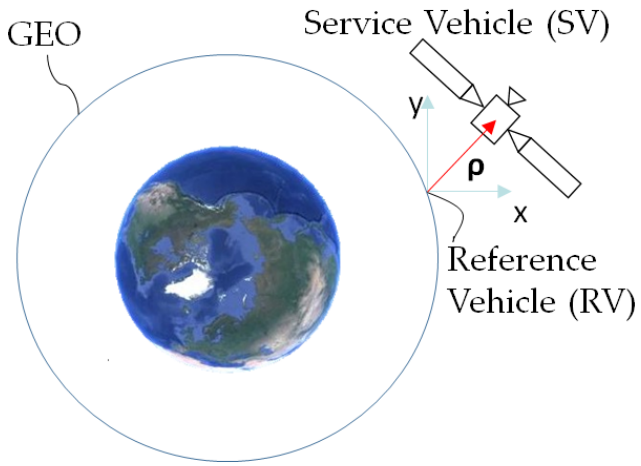

Figure 2.1: Service Vehicle Relative Motion

position vector of the reference vehicle and $\boldsymbol{r}$ the position vector of the service vehicle in an ECI reference frame, by subtracting the two we can obtain the relative position of the service vehicle with respect to the reference spacecraft, as shown in Figure 2.1. The dynamics of the relative motion of the service vehicle, now centered on the reference vehicle, is described by the following equation:

$$\boldsymbol{\delta\ddot{r}}(t) = -\frac{\mu}{r(t)^3}\boldsymbol{r}(t) + \frac{\mu}{r^{*3}}\boldsymbol{r^*}(t) + \frac{\boldsymbol{F}(t)}{m} \tag{2.3}$$

The assumptions made allow us to make use of the CW equations that reduce the dynamics of the problem to be linear which will turn out to be extremely useful for our purpose. As the mission goal is to perform a survey orbit, the relative distance will never grow indefinitely (will actually remain modest), therefore it is possible to linearize Eq. (2.3) and to neglect the higher order terms (H.O.T.). Moreover, since the orbit of the reference vehicle is circular, the mean motion n is constant and given by:

$$n = \sqrt{\frac{\mu}{r^{*3}}} \tag{2.4}$$

Now writing the equations of motion in a rotating reference frame that is centered on the reference spacecraft, and normalizing by proper constants, it is possible to obtain the normalized CW equations that will be used for the remaining of this work.

$$\dot{\boldsymbol{x}}(\tau) = A\boldsymbol{x}(\tau) + B\boldsymbol{u}(\tau) \tag{2.5}$$

where:

$$A = \begin{bmatrix} 0 & 0 & 1 & 0 \\ 0 & 0 & 0 & 1 \\ 3(nT)^2 & 0 & 0 & 2nT \\ 0 & 0 & -2nT & 0 \end{bmatrix} \tag{2.6}$$

$$B = \frac{FT^2}{mS} \begin{bmatrix} 0_{2x2} \\ I_{2x2} \end{bmatrix} \tag{2.7}$$

In Eq. (2.5), $\dot{\boldsymbol{x}}$ is the derivative of the service spacecraft state (relative to the reference spacecraft) with respect to the normalized time τ as opposed to Eq. (2.3) where the derivative is instead with respect to the physical time t. In Eq. (2.6) and (2.7), S and T are normalization constants, n is the

reference spacecraft mean motion, m and F are the service spacecraft mass and maximum thrust. Normalization has the function of enhancing numerical stability as the spacecraft position, velocity and control inputs have all different order of magnitudes, which may cause instabilities if not properly handled. For the problem at hand, S is in the order of hundreds of meters and is equal to the initial separation between service and reference vehicles, $T = 60\,s$, $F = 0.1\,N$, $m = 500\,kg$ and $n = 7.2922\text{e}{-5}\,rad/s$.

The reader should note that only the planar components of the state are considered. In fact, the initial conditions of the service spacecraft are such that it is leading the reference vehicle on the same orbit (phase lead). Although for this particular case, the maneuvers will be coplanar with the orbit plane, the approach adopted in this work can be easily extended to out of plane maneuvers.

Chapter 3

Homotopy Approach

3.1 Mapping Cost Function

As already anticipated, the objective of this work is to find the control history of the service spacecraft that optimizes the fuel consumption while performing a survey orbit of a reference vehicle. In other words, we aim at minimizing the following cost function:

$$J = \tilde{k}(\tau_f, \boldsymbol{x}) + \int_{\tau_0}^{\tau_f} U(\tau) d\tau \tag{3.1}$$

where U, $\tilde{k}$, τ, and $\boldsymbol{x}$ are the normalized thrust magnitude, the vector of the hard terminal constraints, the normalized time and the service spacecraft state vector respectively.

It is well known that the vast majority of optimal control problem must be reduced to a two point boundary value problem (TPBVP) where a system of nonlinear equations has to be solved. With very few exceptions, solving the TPBVP numerically is extremely hard as the convergence is local and strongly dependent on the initial guess provided to solver, moreover, the region of convergence is often extremely small. Therefore, the vast majority of optimal control problems is seldom solved using brute force but rather adopting different, clever approaches.

The linearity of the problem at hand allows for some interesting considerations. In fact, it is well known that a control strategy, illustrated in Eq. (3.3), that makes use of the controllability Gramian of the system, defined in Eq. (3.2), is the solution for the energy optimal problem.

$$W(t_0, t_f) = \int_{t_0}^{t_f} \Phi_A(t_0, \sigma) B B^T \Phi_A^T(t_0, \sigma) d\sigma \tag{3.2}$$

$$\boldsymbol{u^*}(t) = B^T \Phi_A^T(t_0, t) W^{-1}(t_0, t_f) \Big[\Phi_A(t_0, t_f) \boldsymbol{x_f} - \boldsymbol{x_0} \Big] \tag{3.3}$$

where $\Phi_A(t, t_0)$ is the state transition matrix of the system described by Eq. (2.5), $\boldsymbol{x_0} = \boldsymbol{x}(t_0)$ and $\boldsymbol{x_f} = \boldsymbol{x}(t_f)$ are respectively the initial and the final state of the considered arc of trajectory.

In the present work, the approach is to use the analytical solution to the energy optimal problem, obtained through the controllability Gramian and bridge it to the fuel optimal solution through homotopy.

The first step is to express the cost function J of the problem in function of the homotopy parameter ϵ.

$$J = \tilde{k}(\tau_f, \epsilon) + \int_{\tau_0}^{\tau_f} (1 - \epsilon) U(\tau)^2 + \epsilon U(\tau) d\tau \tag{3.4}$$

It is clear that when $\epsilon = 0$, the cost will represent an energy optimal problem while when $\epsilon = 1$, the cost will describe a fuel optimal problem.

An expert eye may already notice that the mapping function proposed in (3.4) will cause problems down the road as it will make the problem singular. This problem has been recognised in [3] where the authors propose a new

mapping function:

$$J = \tilde{k}(\tau_f, \epsilon) + \int_{\tau_0}^{\tau_f} \epsilon U(\tau) + (1-\epsilon)\Big\{U(\tau)\ln\big[U(\tau)\big] + \big[1-U(\tau)\big]\ln\big[1-U(\tau)\big]\Big\}d\tau \tag{3.5}$$

Eq. (3.5) avoids the singularity with the result of having a faster and more accurate solver. However, (3.5) does not fit our needs as we could not make use of the analytical energy optimal solution as a starting point for our optimization. Moreover, the problem defined by (3.4) becomes singular when $\epsilon = 1$ which is our arriving point, so, to avoid the singularity, it is sufficient to stop our integration at a small number like $\epsilon = 1\text{e}{-6}$, which will give a solution that is virtually the same as the fuel optimal solution sought.

3.2 Optimal Control Problem

The Hamiltonian for the stated problem is given by:

$$H(\boldsymbol{p}, \tau) = \boldsymbol{p}^T(A\boldsymbol{x} + B\boldsymbol{\alpha}U) - (1-\epsilon)U^2 - \epsilon U \tag{3.6}$$

where $\boldsymbol{p} = \begin{bmatrix} \boldsymbol{p_s} \\ \boldsymbol{p_v} \end{bmatrix} \in \mathbb{R}^{4x1}$ are the costates of the optimal control problem.

By making use of Pontryagin maximum principle it is possible to find the optimal direction and normalized thrust magnitude, which are given by:

$$\boldsymbol{\alpha} = \frac{\boldsymbol{p_v}}{\|\boldsymbol{p_v}\|} \tag{3.7}$$

$$U^* = \begin{cases} 1 & \text{if } SF > 2-\epsilon \\ 0 & \text{if } SF < \epsilon \\ \frac{SF-\epsilon}{2(1-\epsilon)} & \text{elsewhere} \end{cases} \tag{3.8}$$

where the optimal control input for the continuous thrust case has been obtained by setting $\frac{\partial H}{\partial U} = 0$, and the switching function SF is given by:

$$SF = \frac{FT^2}{mS} \|\boldsymbol{p_v}\| \tag{3.9}$$

In writing (3.7) we are assuming that the only way $\boldsymbol{p_v} = \mathbf{0}$ is if at some time t $\boldsymbol{p} = \mathbf{0}$, which will never happen.

From the formulation of the problem we can see that both the optimal direction and thrust magnitude are function of the costates. Therefore the objective is to find the costates that minimize the cost function J.

The optimal costates must satisfy the Euler-Lagrange equations. The hard terminal constraint can be expressed as:

$$\tilde{k}(\tau_f, \epsilon) = \boldsymbol{\nu}^T(\boldsymbol{x}(\tau_f, \epsilon) - \boldsymbol{x_f}) \tag{3.10}$$

where $\boldsymbol{\nu}$ is the vector of Lagrange multipliers associated with each equality constraint and $\boldsymbol{x_f} = \boldsymbol{x_0}$ since the mission is to perform a surveying orbit of the reference spacecraft.

The Euler-Lagrange equations are given by:

$$\dot{\boldsymbol{p}} = -H_x^T = -A^T\boldsymbol{p} \tag{3.11}$$

$$\boldsymbol{p}(\tau_f) = -\tilde{k}_x^T(\tau_f, \epsilon) = -\boldsymbol{\nu} \tag{3.12}$$

Since the dynamics equations for the costates are the adjunct system of the dynamics of our problem, it is easy to obtain:

$$\boldsymbol{p}(\tau) = -\Phi_A^T(\tau_f, \tau)\boldsymbol{\nu} \tag{3.13}$$

3.3 Stabilized Continuation

The shooting function that needs to be satisfied by the optimal solution is defined by:

$$\boldsymbol{f}[\boldsymbol{\nu}(\epsilon), \epsilon] = \boldsymbol{x}(\tau_f, \epsilon, \boldsymbol{\nu}) - \boldsymbol{x_f} = \boldsymbol{0} \tag{3.14}$$

where

$$\boldsymbol{x}(\tau_f, \epsilon, \boldsymbol{\nu}) = \Phi_A(\tau_f, \tau_0)\left(\boldsymbol{x_0} + \int_{\tau_0}^{\tau_f} \Phi_A(\tau_0, \sigma) B \frac{\boldsymbol{p_v}(\boldsymbol{\nu}(\sigma))}{\|\boldsymbol{p_v}(\boldsymbol{\nu}(\sigma))\|} U^*(\boldsymbol{\nu}(\sigma), \epsilon) d\sigma\right) \tag{3.15}$$

A technique known as stabilized continuation will be adopted to track the zero curve expressed by Eq. (3.14) while bringing ϵ from 0 to 1.

Now that the problem has been completely defined, it is clear that the zero curve expressed by Eq. (3.14) is function of the vector of the Lagrange multipliers $\boldsymbol{\nu}$ and the homotopy parameter ϵ. Therefore, taking its total derivative with respect to the homotopy parameter ϵ we obtain:

$$\frac{d\boldsymbol{f}}{d\epsilon} = \frac{\partial \boldsymbol{f}}{\partial \boldsymbol{\nu}} \frac{\partial \boldsymbol{\nu}}{\epsilon} + \frac{\partial \boldsymbol{f}}{\partial \epsilon} = 0 \tag{3.16}$$

from which it is very easy to obtain the following system of ODEs:

$$\frac{\partial \boldsymbol{\nu}}{\epsilon} = -\frac{\partial \boldsymbol{f}}{\partial \boldsymbol{\nu}}^{-1} \frac{\partial \boldsymbol{f}}{\partial \epsilon} \tag{3.17}$$

As the system of ODEs needs to be integrated numerically, numerical errors will accumulate and propagate throughout the process. In order to ensure to find the final costates that satisfy the shooting function, a stabilizing input has been introduced to (3.17) to ensure exponential stability of the shooting

function error:

$$\frac{\partial \boldsymbol{\nu}}{\epsilon} = -\frac{\partial \boldsymbol{f}}{\partial \boldsymbol{\nu}}^{-1}\Big(\frac{\partial \boldsymbol{f}}{\partial \epsilon} + k\boldsymbol{f}\Big) \tag{3.18}$$

where $k = 100$. To further improve the stability of Eq. (3.18) and be sure to have a shooting function that is as close to 0 as possible when $\epsilon = 1$, an additional stabilizing input that makes use of the controllability Gramiam of the stabilized linear system described by the total derivative of the shooting function has been used.

Indeed, if we add an additional stabilizing input to Eq. (3.18), it can be rewritten as:

$$\frac{d\boldsymbol{f}}{d\epsilon} = -k\boldsymbol{f} + \boldsymbol{\xi}(\epsilon) \tag{3.19}$$

By using the following stabilizing input we can be sure of having a zero shooting function when $\epsilon = 1$ (in the absence of numerical errors):

$$\boldsymbol{\xi}(\epsilon) = -\tilde{\Phi}^T(\epsilon_0, \epsilon)W^{-1}(\epsilon_0, \epsilon_f)\boldsymbol{f}(\boldsymbol{\nu_0}, \epsilon_0) \tag{3.20}$$

where $\tilde{\Phi}^T(\epsilon_0, \epsilon)$ and $W(\epsilon_0, \epsilon_f)$ are the state transition matrix and the controllability Gramian of Eq. (3.19) respectively.

It is easy to show that by substituting Eq. (3.20) inside the solution at ϵ_f to Eq. (3.19) we obtain:

$$\boldsymbol{f}(\boldsymbol{\nu_f}, \epsilon_f) = \tilde{\Phi}(\epsilon_f, \epsilon_0)\boldsymbol{f}(\boldsymbol{\nu_0}, \epsilon_0) - \tilde{\Phi}(\epsilon_f, \epsilon_0)W(\epsilon_0, \epsilon_f)W^{-1}(\epsilon_0, \epsilon_f)\boldsymbol{f}(\boldsymbol{\nu_0}, \epsilon_0) = 0 \tag{3.21}$$

Therefore to system that needs to be integrated in order to obtain the fuel optimal solution to our problem is:

$$\frac{\partial \boldsymbol{\nu}}{\epsilon} = -\frac{\partial \boldsymbol{f}}{\partial \boldsymbol{\nu}}^{-1}\Big(\frac{\partial \boldsymbol{f}}{\partial \epsilon} + k\boldsymbol{f} + \tilde{\Phi}^T(\epsilon_0, \epsilon)W^{-1}(\epsilon_0, \epsilon_f)\boldsymbol{f}(\boldsymbol{\nu_0}, \epsilon_0)\Big) \tag{3.22}$$

For (3.22) to be integrated, partials of the shooting function with respect to $\boldsymbol{\nu}$ and ϵ are to be provided. By making use of the linearity property of integrals and of Leibnitz rule, the sought partials are found from (3.14) and are given by:

$$\frac{\partial \boldsymbol{f}}{\partial \epsilon} = \frac{FT^2}{mS} \int_{\tau_0}^{\tau_f} \Phi_A(\tau_f, \sigma) \begin{bmatrix} 0_{2x2} \\ I_{2x2} \end{bmatrix} \frac{\boldsymbol{p_v}(\boldsymbol{\nu}(\sigma))}{\|\boldsymbol{p_v}(\boldsymbol{\nu}(\sigma))\|} \frac{\partial U(\sigma)^*}{\partial \epsilon} d\sigma \tag{3.23}$$

where

$$\frac{\partial U^*}{\partial \epsilon} = \begin{cases} 0 & \text{if} SF > 2 - \epsilon \\ 0 & \text{if} SF < \epsilon \\ \frac{SF-1}{2(1-\epsilon)^2} & \text{elsewhere} \end{cases} \tag{3.24}$$

and

$$\frac{\partial \boldsymbol{f}}{\partial \boldsymbol{\nu}} = \frac{FT^2}{mS} \int_{\tau_0}^{\tau_f} \Phi_A(\tau_f, \sigma) \begin{bmatrix} 0_{2x2} \\ I_{2x2} \end{bmatrix} \frac{\partial}{\partial \boldsymbol{\nu}} \left[\frac{\boldsymbol{p_v}(\boldsymbol{\nu}(\sigma)) U^*}{\|\boldsymbol{p_v}(\boldsymbol{\nu}(\sigma))\|} \right] d\sigma \tag{3.25}$$

where

$$\frac{\partial}{\partial \boldsymbol{\nu}} \left[\frac{\boldsymbol{p_v} U^*}{\|\boldsymbol{p_v}\|} \right] = \begin{cases} \left[\frac{I}{\|\boldsymbol{p_v}\|} - \frac{\boldsymbol{p_v} \boldsymbol{p_v}^T}{\|\boldsymbol{p_v}\|^3} \right] \frac{\partial \boldsymbol{p_v}}{\partial \nu} & \text{if} SF > 2 - \epsilon \\ 0 & \text{if} SF < \epsilon \\ \left[\frac{U^* I}{\|\boldsymbol{p_v}\|} + \frac{\epsilon \boldsymbol{p_v} \boldsymbol{p_v}^T}{2(1-\epsilon)\|\boldsymbol{p_v}\|^3} \right] \frac{\partial \boldsymbol{p_v}}{\partial \nu} & \text{elsewhere} \end{cases} \tag{3.26}$$

$$\frac{\partial \boldsymbol{p_v}(\sigma)}{\partial \boldsymbol{\nu}} = -\Phi_A(\tau_f, \sigma)^T \tag{3.27}$$

3.4 Zero Curve Tracking

Although the algorithm proposed should guarantee the tracking of the zero curve represented by the shooting function in Eq. (3.14), the present formulation presents a singularity at $\epsilon = 1$. Therefore, the closer we get to the fuel optimal solution, the harder it becomes to overcome the numerical error. In order to improve the precision to which the shooting function is satisfied, the following method to enhance the zero curve tracking is proposed.

The structure of the proposed algorithm is in part very similar to Kalman filters, as it is divided in a prediction step, where the optimal costates at final time are propagated, and in a correction step, where the costates and the homotopy parameter are corrected with the objective of minimizing the residuals of the shooting function.

The prediction step is performed by integrating Eq. (3.22) using MATLAB ode45, however the span of integration $\epsilon \in [0, 1]$ is divided in a number of subintervals which in general has to be determined heuristically. In the present work, we considered 10 subintervals.

The correction step takes place at the end of each subinterval. In order to find the required correction let us define $\boldsymbol{z} = [\boldsymbol{\nu}^T, \epsilon]^T$ and expand Eq. (3.14) in Taylor series:

$$\boldsymbol{f}(\boldsymbol{z} + \boldsymbol{\Delta z}) = \boldsymbol{f}(\boldsymbol{z}) + \frac{d\boldsymbol{f}}{d\boldsymbol{z}}\boldsymbol{\Delta z} + H.O.T. \tag{3.28}$$

Since our objective is to bring $\boldsymbol{f}(\boldsymbol{z})$ to $\mathbf{0_{4x1}}$ and $\frac{d\boldsymbol{f}}{d\boldsymbol{z}} = \left[\frac{\partial \boldsymbol{f}}{\partial \boldsymbol{\nu}}, \frac{\partial \boldsymbol{f}}{\partial \epsilon}\right]$, inverting Eq. (3.28) we obtain the correction we are looking for:

$$\boldsymbol{\Delta z} = -\left[\frac{\partial \boldsymbol{f}}{\partial \boldsymbol{\nu}}, \frac{\partial \boldsymbol{f}}{\partial \epsilon}\right]^{+} \boldsymbol{f}(\boldsymbol{z}) \tag{3.29}$$

where $[\bullet]^+$ represents the Moore-Penrose pseudoinverse.

The correction step is an iterative process in which the vector $\boldsymbol{z}$ is updated, following the update law of Eq. (3.30), until $\|\boldsymbol{\Delta z}\|$ is smaller than a predetermined tolerance value.

$$\boldsymbol{z}^{(n+1)} = \boldsymbol{z}^{(n)} + \boldsymbol{\Delta z} \tag{3.30}$$

Two observations are in order here. In an effort to speed up the homotopy bridging, the correction step can be truncated if convergence is not reached after an appropriate number of steps. Eq. (3.29) follows the assumption of negligible H.O.T., and for this assumption to be valid, a trust region on the selection of $\boldsymbol{\Delta z}$ needs to be used. The trust region that has been used in this work is given by:

$$TR = min\Big(1, \frac{\|\boldsymbol{z}\|}{\|\boldsymbol{\Delta z}\|}1\text{e}{-3}\Big) \tag{3.31}$$

3.5 Extension to 3D Maneuvers

Extendind the problem to 3D and leaving everything the same is straightforward as it is enough to change the matrices A and B to:

$$A = \begin{bmatrix} & 0_{3x3} & & & I_{3x3} & \\ 3(nT)^2 & 0 & 0 & 0 & 2nT & 0 \\ 0 & 0 & 0 & -2nT & 0 & 0 \\ 0 & 0 & -(nT)^2 & 0 & 0 & 0 \end{bmatrix} \tag{3.32}$$

$$B = \frac{FT^2}{mS}\begin{bmatrix} 0_{3x3} \\ I_{3x3} \end{bmatrix} \tag{3.33}$$

However, we can slightly modify the present formulation in order to improve accuracy at the expenses of the convergence speed. The improvement will be the same as the one proposed in [5] which is to constrain the constates at final time to a 7D unit sphere.

If we premultiply (3.4) by a constant p_0 the problem does not change. At this point by rewriting the Hamiltonian for the new cost function we can see that both the Hamiltonian and Euler-Lagrange equations are homogeneous

in the components of the augmented costates vector $\boldsymbol{p} = \begin{bmatrix} p_0 & \boldsymbol{p_x}^T & \boldsymbol{p_v}^T \end{bmatrix}$ which can therefore be normalized by multiplying and dividing by its norm.

The optimization variables now form the vector $\boldsymbol{\chi} \in \Re^{6x1}$ where $\chi_i \in [0,1]$. We can now form the vector $\boldsymbol{\beta} = \begin{bmatrix} \frac{\pi}{2}\boldsymbol{\chi}_{1,2}^T & \pi(\boldsymbol{\chi}_{3,4}^T - \frac{1}{2}) & 2\pi\boldsymbol{\chi}_{5,6}^T \end{bmatrix}$ which fully define the normalized costates at final time which will be given by $\bar{\boldsymbol{p}} = \begin{bmatrix} \bar{p_0} & \bar{\boldsymbol{p}}_{\boldsymbol{x}}{}^T & \bar{\boldsymbol{p}}_{\boldsymbol{v}}{}^T \end{bmatrix}^T$, where:

$$\bar{p_0} = \sin\beta_1 \tag{3.34}$$

$$\bar{\boldsymbol{p}}_{\boldsymbol{x}} = \cos\beta_1 \sin\beta_2 \begin{bmatrix} \cos\beta_3\cos\beta_5 & \cos\beta_3\sin\beta_5 & \sin\beta_3 \end{bmatrix}^T \tag{3.35}$$

$$\bar{\boldsymbol{p}}_{\boldsymbol{v}} = \cos\beta_1 \sin\beta_2 \begin{bmatrix} \cos\beta_4\cos\beta_6 & \cos\beta_4\sin\beta_6 & \sin\beta_4 \end{bmatrix}^T \tag{3.36}$$

The optimal control input will still be given by (3.8), however, the switching function will now be:

$$SF = \frac{FT^2 \left\| \boldsymbol{p_v} \right\|}{\bar{p_0} m S} \tag{3.37}$$

Finally the partial derivatives of the shooting function (3.14) with respect to ϵ remains unchanged while the one with respect to the new optimization variable $\boldsymbol{\chi}$ is given by:

$$\frac{\partial \boldsymbol{f}}{\partial \boldsymbol{\chi}} = \frac{FT^2}{mS} \int_{\tau_0}^{\tau_f} \Phi_A(\tau_f, \sigma) \begin{bmatrix} 0_{3x3} \\ I_{3x3} \end{bmatrix} \frac{\partial}{\partial \boldsymbol{\chi}} \left[\frac{\boldsymbol{p_v}(\boldsymbol{\chi}(\sigma)) U^*}{\left\| \boldsymbol{p_v}(\boldsymbol{\chi}(\sigma)) \right\|} \right] d\sigma \tag{3.38}$$

where

$$\frac{\partial}{\partial \boldsymbol{\chi}} \left[\frac{\boldsymbol{p_v} U^*}{\left\| \boldsymbol{p_v} \right\|} \right] = \begin{cases} -\frac{[\boldsymbol{p_v}\times]^2}{\left\| \boldsymbol{p_v} \right\|^3} \frac{\partial \boldsymbol{p_v}}{\partial \chi} & \text{if } SF > 2 - \epsilon \\ 0 & \text{if } SF < \epsilon \\ \frac{1}{2(1-\epsilon)\left\| \boldsymbol{p_v} \right\|} \left[\frac{\epsilon [\boldsymbol{p_v}\times]^2}{\left\| \boldsymbol{p_v} \right\|^2} + SFI \right] \frac{\partial \boldsymbol{p_v}}{\partial \chi} - \frac{SF \boldsymbol{p_v}}{2\bar{p_0}(1-\epsilon)} \frac{\partial \bar{p_0}}{\partial \chi} & \text{elsewhere} \end{cases} \tag{3.39}$$

and

$$\frac{\partial \boldsymbol{p_v}}{\partial \boldsymbol{\chi}} = \frac{\partial \boldsymbol{p_v}}{\partial \boldsymbol{\beta}} \frac{\partial \boldsymbol{\beta}}{\partial \boldsymbol{\chi}} \tag{3.40}$$

$$\frac{\partial \bar{p}_0}{\partial \boldsymbol{\chi}} = \begin{bmatrix} \cos\beta_1 & \mathbf{0_{1x5}} \end{bmatrix} \frac{\partial \boldsymbol{\beta}}{\partial \boldsymbol{\chi}} \tag{3.41}$$

$$\frac{\partial \boldsymbol{\beta}}{\partial \boldsymbol{\chi}} = diag \begin{bmatrix} \frac{\pi}{2} I_{2x2} & \pi I_{2x2} & 2\pi I_{2x2} \end{bmatrix} \tag{3.42}$$

Chapter 4

Energy Optimal Solutions

For the present work, three mission profiles have been considered and with the use of Eq. (3.3) it was possible to perform a reachability analysis and a trade study for all of them. The mission profiles selected are summarized in Table 4.1, and are all representative of real missions needs.

Table 4.1: Mission Profiles Description.

Mission Profile Identification	**Mission Profile Description**
MP1	phase angle change
MP2	survey orbit
MP3	survey orbit with no fly zone

The MP3 is likely to be the preferred profile for real missions due to safety and operational constraints, however the results of the trade study performed on the others may offer valuable insights on different strategies.

The reachability analysis is very useful as it offers a very quick visualization on the feasibility of a given profile as well as on the feasibility to bridge a given energy optimal solution with the corresponding fuel optimal solution. Examples of reachability analyses (with respect to time of flight and phase lag intercept) are shown in Figure 4.1a and Figure 4.1b, where a constrained

survey orbit has been considered with initial separation of 200 meters. On the reachability analysis presented in Figure 4.1a, the phase lag intercept has been fixed to 200 meters, while the time of flight of Figure 4.1b has been fixed to 140 minutes. In the following, for illustrative purpose, a no fly zone of the

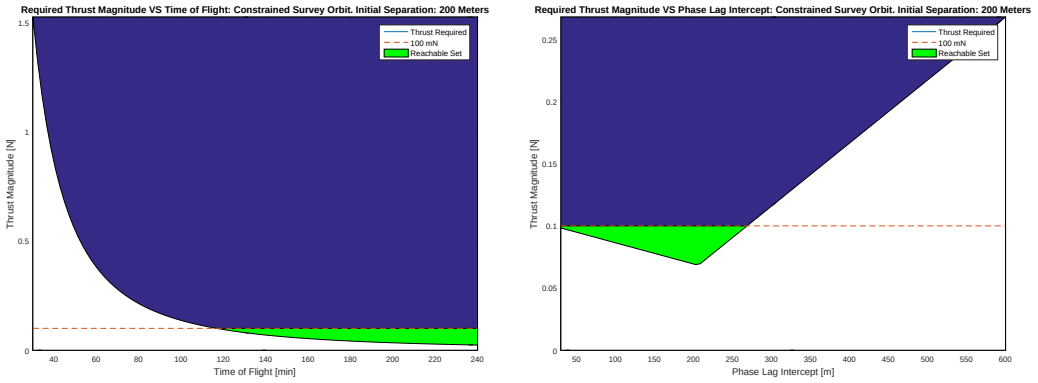

(a) (b)

Figure 4.1: (a): Reachable Set for Constrained Survey Orbit with respect to Time of Flight. (b): Reachable Set for Constrained Survey Orbit with respect to Phase Lag Intercept

form of a 30 meters radius ball has been considered. The ball can be made arbitrarily large without loss of generality.

4.1 Mission Profile 1: Phase Angle Change

In order to aid the understanding of the topology of mission profile 1, Figure 4.2 shows a sketch of such a scenario. In this scenario, the mission is to from phase lead to phase lag with respect to the reference spacecraft without worrying about any no fly zone.

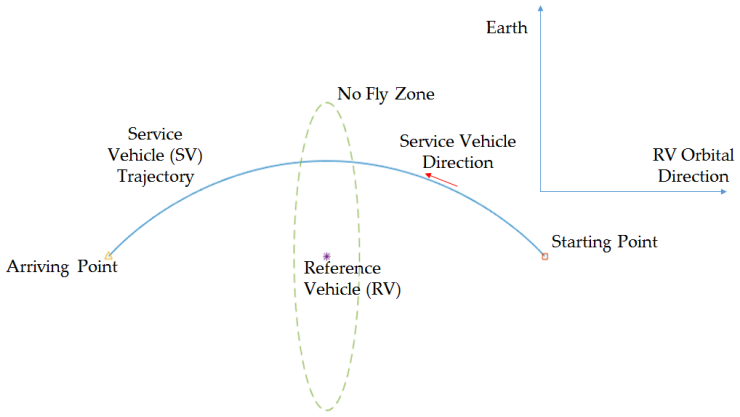

Figure 4.2: Mission Profile 1 Sketch

In order to use Eq. (3.3) effectively, a target point needs to be selected. For MP1 the target point is such that the lag angle at final time is the same as the lead angle at initial time. The trade study was performed varying initial separation between reference and service vehicle and time of flight, the results are showed in Figure 4.3a and Figure 4.3b. The plots show only the results

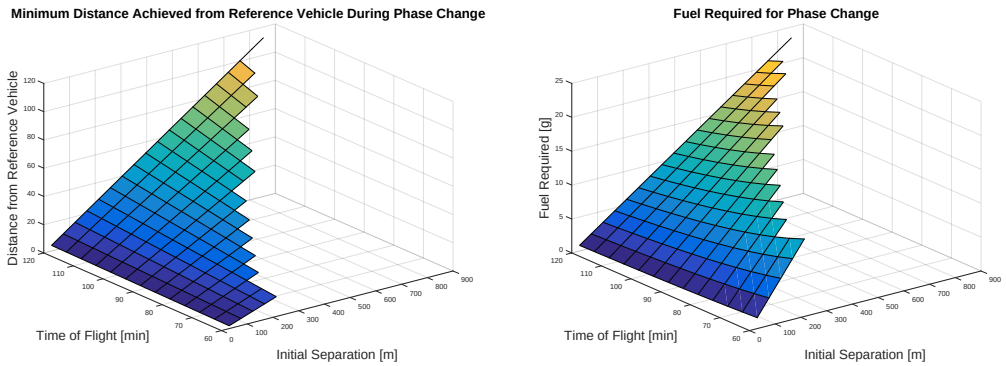

(a) (b)

Figure 4.3: (a): Minimum Distance Achieved During Phase Angle Change. (b): Fuel Required for Phase Angle Change

which are reachable with a thrust authority smaller than or equal to $100\,mN$. It should not come as a surprise that the larger the initial separation and the shorter the time of flight, the more fuel will be required. The same goes for the minimum distance achieved from the reference vehicle where the larger the initial separation and time of flight, the larger the minimum distance will be. Figure 4.4 shows an example trajectory for a scenario in which the no fly zone is not violated.

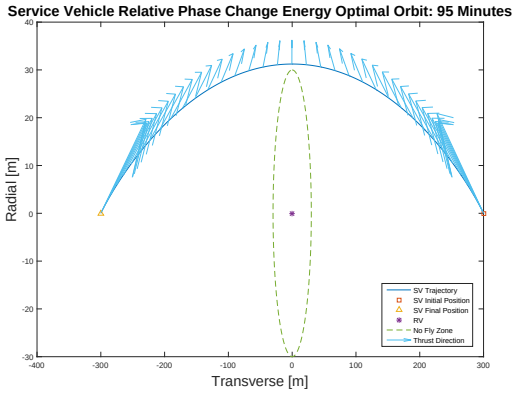

Figure 4.4: Phase Angle Change Example Trajectory

4.2 Mission Profile 2: Unconstrained Survey Orbit

Figure 4.5 shows a sketch for MP2 where the mission is to do a survey orbit of the reference spacecraft. Again no constraints are imposed in the trajectory of the service vehicle. The procedure to find the control input history for MP2 is similar to the one adopted previously with two main differences. The service spacecraft will now need to go back to its starting position,

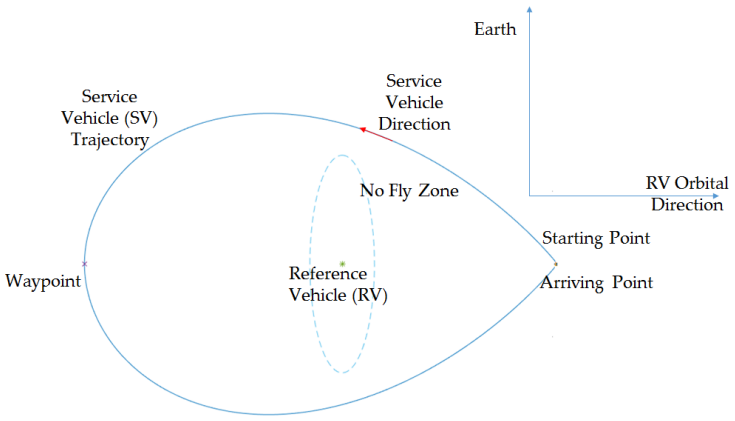

Figure 4.5: Mission Profile 2 Sketch

therefore a waypoint located halfway needs to be provided. Moreover, for the maneuver to be realizable, continuity in the control input is necessary.

Since initial and final states are assigned, as well as the position vector of the waypoint, the velocity of the service spacecraft at the waypoint are our only degrees of freedom (two since the problem is planar) which we need to select properly in order to make the spacecraft trajectory continuous. This is done by imposing the control input just before the waypoint to be equal to the one just after it, as described by Eq. (4.1).

$$\boldsymbol{u}^*(t_1)^- = \boldsymbol{u}^*(t_1)^+ \tag{4.1}$$

where $\boldsymbol{u}^*$ is the optimal control input. The quantities expressed in Eq. (4.1) are given by:

$$\boldsymbol{u}^*(t_1)^- = B^T\Phi^T(t_0,t_1)W^{-1}(t_0,t_1)[\Phi(t_0,t_1)\boldsymbol{x^*}(t_1) - \boldsymbol{x_0}] \tag{4.2}$$

$$\boldsymbol{u}^*(t_1)^+ = B^TW^{-1}(t_1,t_f)[\Phi(t_1,t_f)\boldsymbol{x_0} - \boldsymbol{x^*}(t_1)] \tag{4.3}$$

Since $\boldsymbol{x_f} = \boldsymbol{x_0}$ by definition, equating Eq. (4.2) and (4.3) we obtain the system of 2 linear algebraic equations in 2 unknowns, which are the velocity components of $\boldsymbol{x_1}$.

$$K\boldsymbol{x_1} + b\boldsymbol{x_0} = \boldsymbol{0} \tag{4.4}$$

where:

$$K = B^T[\Phi^T(t_0, t_1)W^{-1}(t_0, t_1)\Phi(t_0, t_1) + W^{-1}(t_1, t_f)] \tag{4.5}$$

$$b = -B^T[\Phi^T(t_0, t_1)W^{-1}(t_0, t_1) + W^{-1}(t_1, t_f)\Phi(t_1, t_f)] \tag{4.6}$$

Using the solution to Eq. (4.4) to properly select the waypoint, it was possible to perform a trade study, similarly to what was done for mission profile 1, the results of which will be omitted as they are very similar to what presented for MP1. Figure 4.6 shows instead an example trajectory of an orbit in which the no fly zone is not violated.

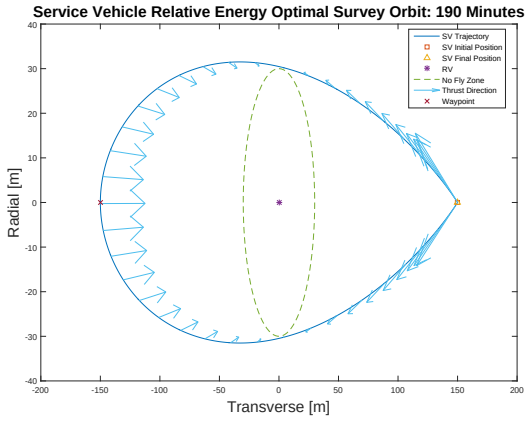

Figure 4.6: Unconstrained Survey Orbit Example Trajectory

4.3 Mission Profile 3: Constrained Survey Orbit

Figure 4.7 shows a sketch for MP3 where the mission is for the service vehicle to perform a survey orbit of the reference vehicle, this time imposing a no fly zone. As already anticipated in the introduction, path constraints

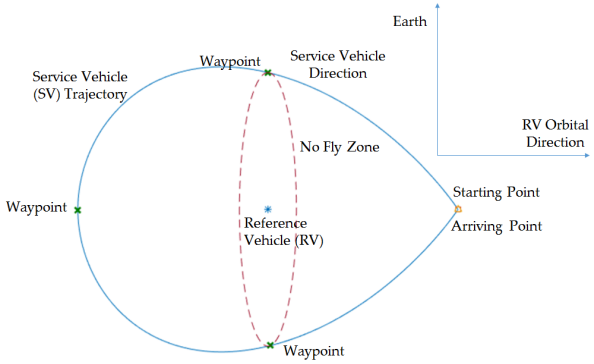

Figure 4.7: Mission Profile 3 Sketch

are hard to handle as they usually ask for a discretization of the problem. At this point, the optimization problem can be solved directly by making use of convex optimization techniques integrated with an MPC approach, or indirectly where the prior knowledge of the sequence of on and off boundary arcs is usually required (and is seldom known).

The approach proposed in this work is rather to implicitly impose the no fly zone by selecting properly two additional waypoints that are symmetric with respect to the x-axis. Again, continuity in the control input is paramount for maneuver feasibility. The approach followed is equal in nature to the one adopted for mission profile 2, however in this case there will be 6 equations in 6 unknowns as also the velocity of the spacecraft at the two additional

waypoints need to be defined.

A trade off needs to be performed between fuel consumption and violation of no fly zone. Typical energy optimal solutions tend to violate the no fly zone if the ratio between initial separation and minimum distance allowed is too low. Intuition would push us to think that in order to achieve the most fuel efficient energy optimal solution, the constraint waypoints have to be selected just on the boundaries of the no fly zone in the cases where the latter would be violated on the unconstrained energy optimal trajectory. The following trade study shows that this intuition is correct. Figure 4.8a shows the fuel

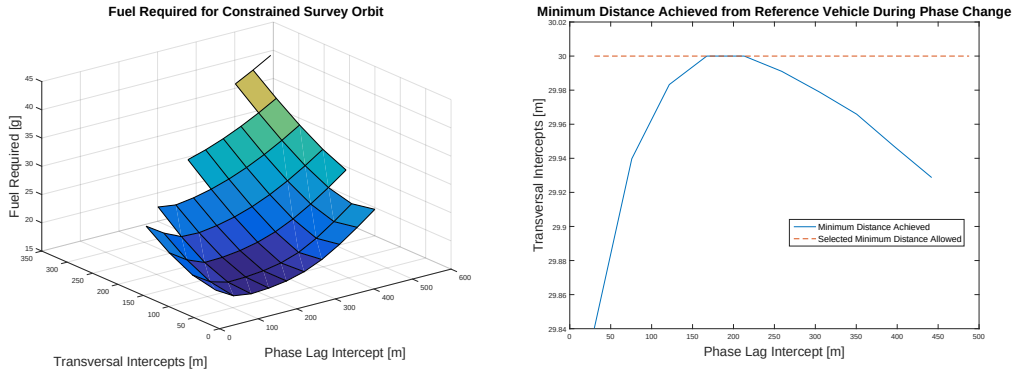

(a) (b)

Figure 4.8: (a): Fuel Consumption Trade Study for Constrained Survey Orbit. (b): Minimum Distance Achieved for Constrained Survey Orbit.

consumption for the survey orbit for a given time of flight (190 minutes) and different transversal intercepts (y-axis intercepts in the trajectory plots) and phase lag intercepts (x-axis intercepts in the trajectory plots). It is clear that the minimum fuel is achieved when the transversal intercepts are just on the

boundaries of the no fly zone.

To complete the picture, another trade study is needed in order to select the phase lag intercept that, while guaranteeing the most fuel efficient energy optimal solution, ensures that the no fly zone is not violated. The result of this trade study can be found in Figure 4.8b.

Cross comparing Figure 4.8a with Figure 4.8b we can see that the most fuel efficient energy optimal solution for a 95 minutes constrained survey orbit is given by putting the transversal intercepts on the boundary of the no fly zone and the phase lag intercept at about 167 meters from the reference spacecraft. Such an orbit is reported on Figure 4.9.

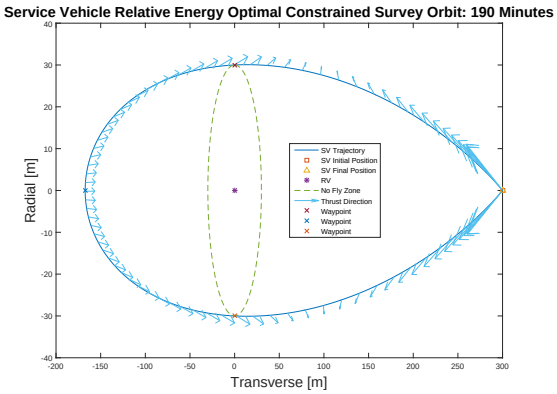

Figure 4.9: Constrained Survey Orbit Example Trajectory

Chapter 5

Fuel Optimal Solutions

The algorithm proposed in this work has proven to be quite effective, as convergence has always been achieved, for mission profiles 1 and 2. However, the singularity that is embedded in the proposed formulation poses considerable difficulties in the satisfaction of the shooting function with high precision. In fact, the proposed algorithm is able to reduce the residuals only to the relatively low order of accuracy of 1e−4, which corresponds to an accuracy at the centimeter level. The implementation of the proposed zero curve tracking algorithm, improved the accuracy of the homotopy algorithm at the expenses of CPU time. However, the singularity in the problem proved to be cumbersome to handle, therefore further research is needed in this direction. As an example, simulation results for a test case falling inside mission profile 1 is shown in Figure 5.1.

CPU time has been measured with the MATLABs function tic-toc. Twenty test cases have been ran and the results have been averaged. The tests ran revealed that the proposed homotopy algorithm converges in 60.73 seconds when zero curve tracking is off and in 185.28 seconds when zero curve tracking is on. The proposed approach proved to be ineffective to bridge the

energy optimal solution to the corresponding fuel optimal solution for mission profile 3. However, the relatively little CPU time required allows for some trade studies which will prove to be of great value.

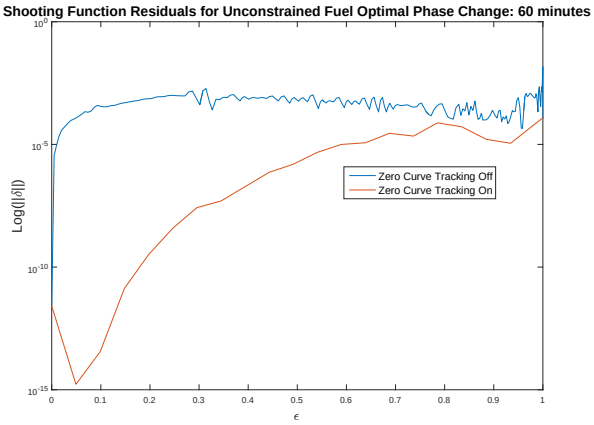

Figure 5.1: Zero Curve Tracking Effect: Test Case

5.1 Mission Profile 1: Phase Angle Change

In order to produce plots that are easier to see and analyze two different trade studies were carried on. The first where time of flight was fixed to 95 minutes and only the initial separation between service and reference vehicles was varied (results showed in Figure 5.2a) and the other where initial separation was fixed to 200 meters and time of flight was varied (results showed in Figure 5.2b). As expected the fuel required by the fuel optimal solutions stays steadily below the fuel required by the energy optimal solutions by a good margin in both cases. Moreover, upon further analysis, we can see that in the

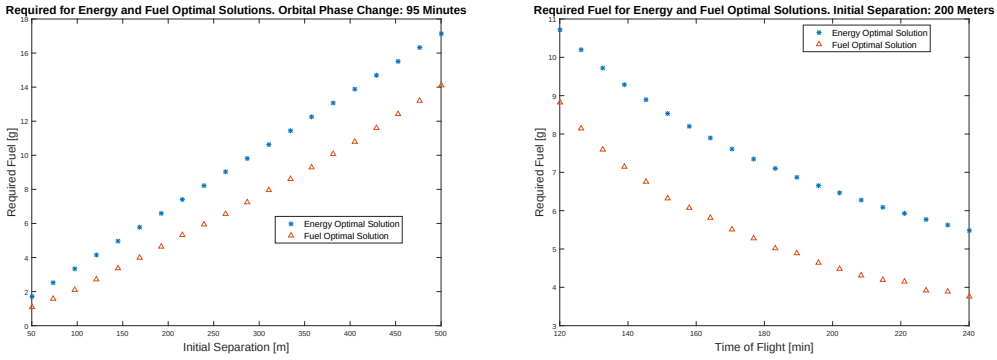

(a) (b)

Figure 5.2: (a): Required Fuel Comparison Between Fuel and Energy Optimal Solutions for Orbital Phase Change VS Service and Reference Vechicles Initial Separation. (b): Required Fuel Comparison Between Fuel and Energy Optimal Solutions for Orbital Phase Change VS Time of Flight.

first case (Figure 5.2a), the saving in fuel varies from 17.5% to 38%, while in the second case the saving in fuel goes from 17.8% to 32.1%.

An interesting pattern emerged when minimum distance from the reference vehicle have been compared on the same plot, as shown in Figure 5.3a and 5.3b. Figures 5.3a and 5.3b show that the fuel optimal solution is always safer than the energy optimal solution for mission profile 1. This is an extremely important characteristic because it ensures that if the no fly zone is not violated by the energy optimal solution, the bridged fuel optimal solution will behave accordingly. An example trajectory will be presented in the following. To produce the following plots, a test case defined by 85 minutes of time of flight and an initial separation of 200 meters. Figure 5.4 shows the sequential homotopy reduction from energy optimal to fuel optimal solution, the reader

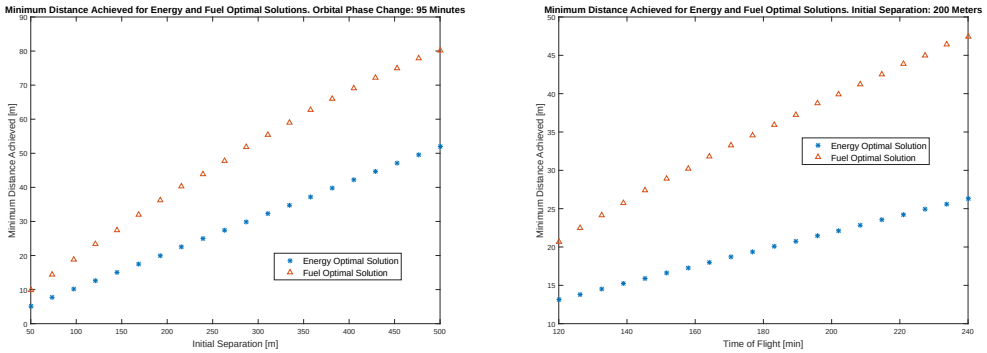

(a) (b)

Figure 5.3: (a): Minimum Distance Achieved Comparison for Orbital Phase Change. (b): Minimum Distance Achieved Comparison for Orbital Phase Change VS Time of Flight.

should not be surprised by the fact that the fuel optimal solution is bang-bang. Figures 5.5a and 5.5b show the fuel optimal trajectory and the comparison between the latter and the corresponding energy optimal trajectory. Figure 5.5b shows how useful is the fact that for MP1, the fuel optimal trajectory is safer than the energy optimal one. In fact, while the latter violates the no fly zone, the former does not, thus satisfying more stringent requirements.

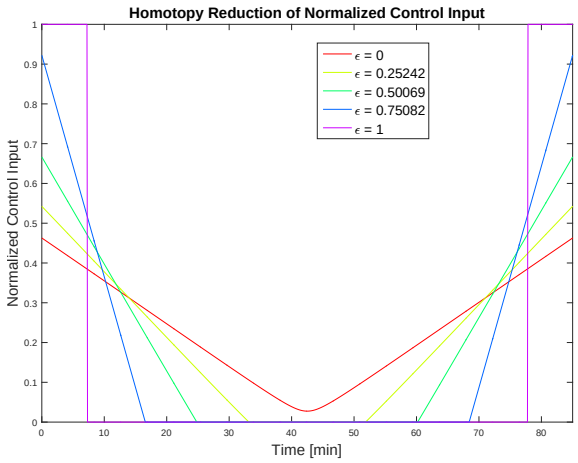

Figure 5.4: Homotopy Reduction for Orbital Phase Change

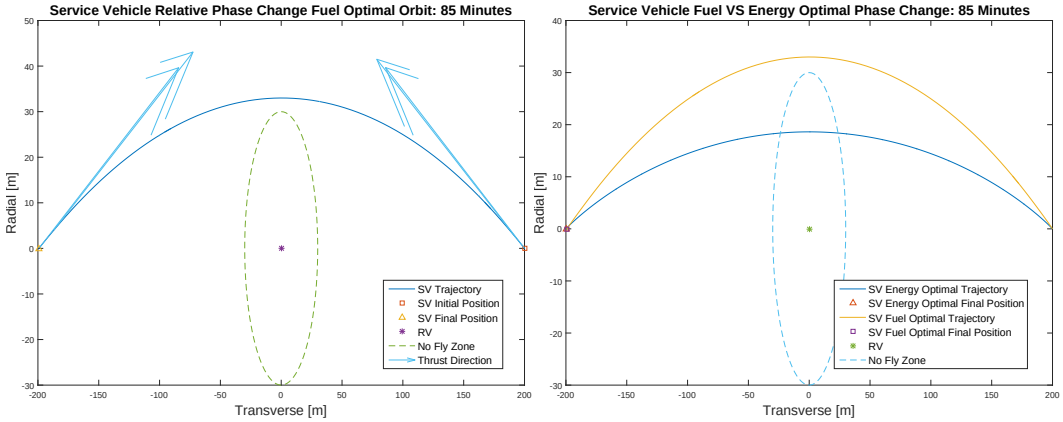

(a) (b)

Figure 5.5: (a): Fuel Optimal Example Trajectory for Orbital Phase Change. (b): Comparison Between Energy and Fuel Optimal Trajectories for Orbital Phase Change.

5.2 Mission Profile 2: Unconstrained Survey Orbit

Following the approach adopted for MP1, a similar trade study has been performed for MP2, for which only the case of varying phase lag intercept will be presented. For Figures 5.6a and 5.6b, a time of flight of 190 minutes has been considered. Figure 5.6a shows that for the MP2 the saving in fuel is between 24.4% and 32.5%. Figure 5.6b shows that for MP2, the fuel optimal

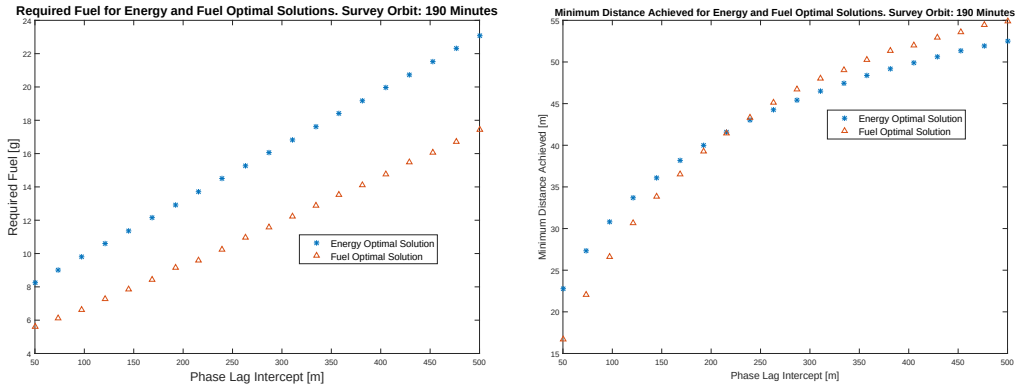

(a) (b)

Figure 5.6: (a): Required Fuel Comparison for Unconstrained Survey Orbit. (b): Minimum Distance Achieved for Unconstrained Survey Orbit.

trajectory is not always safer than the energy optimal trajectory. However, it becomes safer for a phase lag intercept that is further away than the initial separation between reference and service vehicles. A test case with a phase lag intercept of 239 meters (the closest intercept that guarantees a safer fuel optimal orbit) has been considered to show an example of the homotopy reduction and of the resulting trajectory which is summarized by figures 5.7, 5.8a and 5.8b.

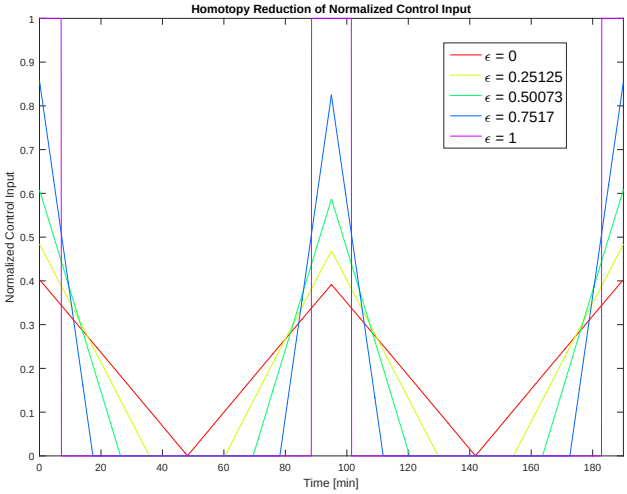

Figure 5.7: Homotopy Reduction for Unconstrained Survey Orbit

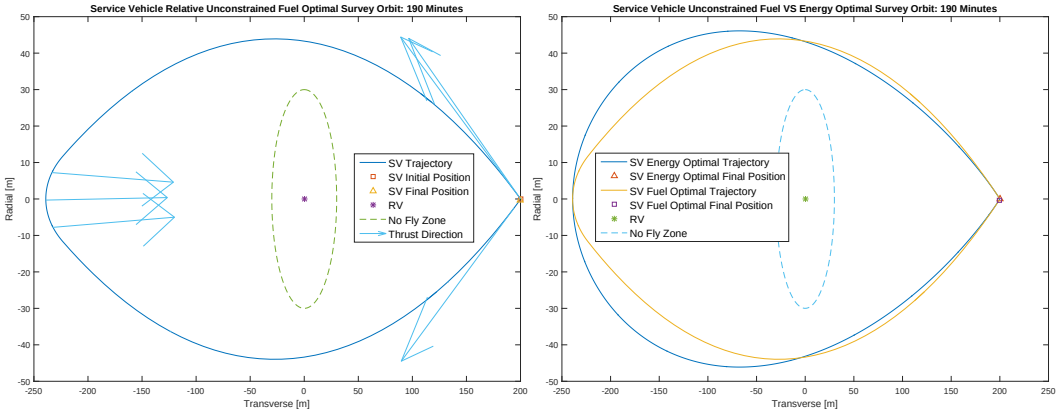

(a) (b)

Figure 5.8: (a): Fuel Optimal Example Trajectory for Unconstrained Survey Orbit. (b): Comparison Between Energy and Fuel Optimal Trajectories for Unconstrained Survey Orbit.

5.3 3D Maneuvers Preliminary Examples

To serve the purpose of illustrating the extendability of appliance of the proposed approach of out of plane maneuvers, some example trajectories have been found by directly applying the approach outlined in paragraph 3.5. First the same scenario that was used in the simulations performed for MP1 was simulated in order to show that adding one dimension does not change the optimal to which the solver converges to. Figures 5.9a and 5.9b show that the fuel optimal trajectory is coplanar with the reference vehicle orbit and that the thrust profile is the same as MP1 in magnitude and direction. This comes at no surprise because the intuition developed for impulsive maneuvers teach us that out of plane maneuvers are more expensive in terms of fuel than in plane maneuvers. Therefore if the arrival point is on the same plane of the initial orbit, there is no necessity to move to another orbital plane.

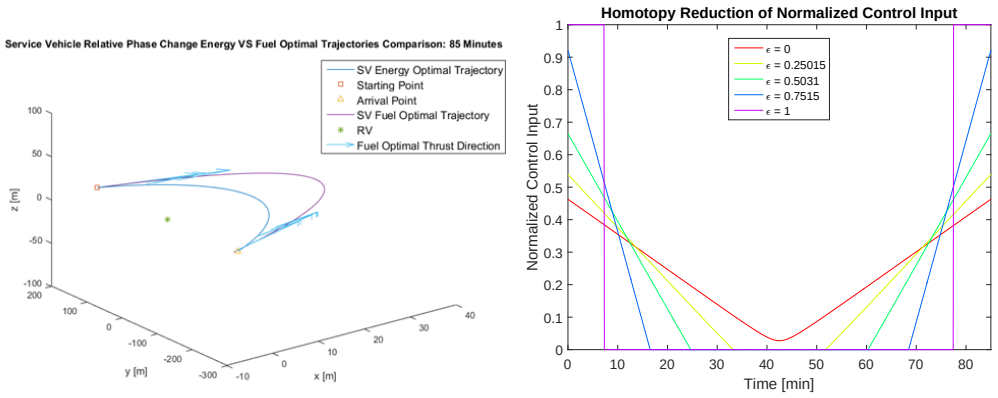

(a) (b)

Figure 5.9: (a): Fuel Optimal Planar Phase Change Maneuver Simulated with 3D Solver (b): Thrust Profile of Planar Phase Change Simulated with 3D solver.

The situation changes if we select as initial and final point locations that out of the orbital plane of the reference vehicle. While figures 5.10a and 5.10b show that the thrust profile remains essentially the same in both magnitude and direction, it is clear that now the maneuver happens in a plane that is not aligned with the orbital plane of the reference vehicle. Further work is needed to improve the accuracy of the 3D extension of the homotopic approach presented and to identify whether there are patterns in the plane of the orbital maneuver and if so, if it is possible to drive conditions to find them analytically.

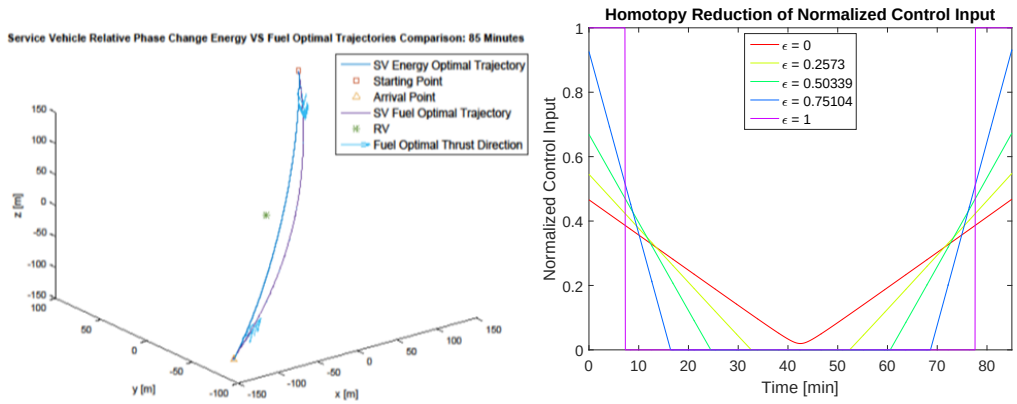

(a) (b)

Figure 5.10: (a): Fuel Optimal 3D Phase Change Maneuver (b): Thrust Profile of 3D Phase Change Simulated.

As concluding remarks, figures 5.11a and 5.11b show that the proposed maneuvers are feasible as the angle between subsequent thrust directions vary with a reasonable rate for spacecraft applications.

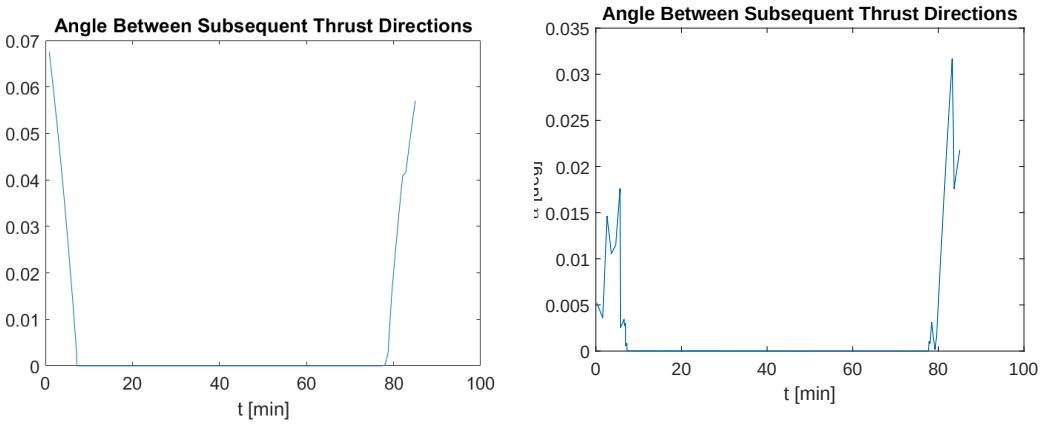

(a) (b)

Figure 5.11: (a): Thrust Angles MP1 (b): Thrust Angles MP4.

Chapter 6

Conclusions

This report presents an innovative approach to bridge analytical energy optimal solutions to the corresponding fuel optimal solutions. Furthermore, an algorithm to ensure higher precision in the convergence of the homotopy method has been also proposed. The author recognized the importance of imposing path constraints when performing proximity operations, however the approach that has been proposed only allows for a soft imposition of the path constraints through waypoints.

All of the simulations have been performed on a machine equipped with 8 GB RAM and an Intel Core i7-3537U 2.50 GHz where hyper-threading could not be disabled (forcing each core to be capped at 50%).

The proposed approach revealed to be inefficient in finding the solution when more than 1 waypoint was imposed which can be a somewhat high limitation. However, the relatively short time to obtain each homotopy reduction allowed for trade studies that offered precious insights on the structure of the fuel optimal compared to the energy optimal solutions. Namely, it has been showed that regions in which fuel optimal solutions are safer than their energy optimal counterparts exist, thus mitigating the inability of the proposed

algorithm to converge in cases in which more than 1 waypoint is needed.

It has been shown that the fuel optimal solutions that have been identified for the test cases considered offer a saving in fuel of minimum 17% and as high as 38% when compared to their energy optimal counterparts.

Future directions for this work are a better integration of the zero curve tracking enhancement to the proposed algorithm in order to improve the convergence accuracy, a relaxation of the assumption of circular orbit in order to consider reference vehicles working in orbits different than GEO and the inclusion of orbital perturbations due to J_2, J_3, third body effects and solar radiation pressure.

Bibliography

[1] R. S. Erwin A. Weiss, M. Baldwin and I. Kolmanovsky. Model predictive control for spacecraft rendezvous and docking: Strategies for handling contraints and case studies. *IEEE Transactions on Control Systems Technology*, 23(4):1638–1647, 2015.

[2] W. H. Clohessy and R. S. Wiltshire. Terminal guidance for satellite rendezvous. *Journal of the Aerospace Sciences*, 27(9):653–674, 1960.

[3] I. Kolmanovsky E. Taheri and E. Atkins. Enhanced smoothing technique for indirect optimization of minimum-fuel low-thrust trajectories. *Journal of Guidance, Control and Dynamics*, 39(11):2500–2511, 2016.

[4] F. Markley et al. Guidance and navigation for rendezvous and proximity operations with a non-cooperative spacecraft at geosynchronous orbit. *George H. Born Symposium*, 2010.

[5] H. Baoyin F. Jiang and J. Li. Practical techniques for low-thrust trajectory optimization with homotopic approach. *Journal of Guidance, Control and Dynamics*, 35(1):245–258, 2012.

[6] P. Sturdza J. R. R. A. Martins and J. J. Alonso. The complex-step derivative approximation. *ACM Transactions on Mathematical Software*, 29(3):245262, 2003.

[7] E. M. Kollin. Autonomous time-optimal spacecraft rendezvous and proximity operations using stabilized continuation. *UT Electronic Theses and Dissertations*, 2016.

[8] G. R. Kotamraju and M. R. Akella. Stabilized continuation methods for boundary value problems. *Applied Mathetmatics and Computation*, 112(2-3):317–332, 2000.

[9] R. R. Kumar and H. Seywald. Fuel-optimal stationkeeping via differential inclusions. *Journal of Guidance, Control and Dynamics*, 18(5):1156–1162, 1995.

[10] J. Li and X. Xi. Fuel-optimal low-thrust reconfiguration of formation-flying satellites via homotopic approach. *Journal of Guidance, Control and Dynamics*, 35(6):1709–1717, 2012.

[11] P. Lu and X. Liu. Autonomous trajectory planning for rendezvous and proximity operations by conic optimization. *Journal of Guidance, Control and Dynamics*, 36(2):375389, 2013.

[12] H. Park S. Di Cairano and I. Kolmanovsky. Model predictive control approach for guidance for guidance of spacecraft rendezvous and proximity maneuvering. *Int. J. Robust. Nonlinear Control*, 22:1398–1427, 2012.

[13] P. Martinon T. Haberkorn and J. Gergaud. Low-thrust minimum-fuel orbital transfer: A homotopic approach. *Journal of Guidance, Control and Dynamics*, 27(6):1046–1060, 2004.